Probing the Ultrafast Energy Dissipation Mechanism of the Sunscreen Oxybenzone after UVA Irradiation

Lewis A. Baker,[1‡] Michael D. Horbury,[1‡] Simon E. Greenough,[1] Philip M. Coulter,[2] Tolga N. V. Karsili,[2] Gareth M. Roberts,[2] Andrew J. Orr-Ewing,[2] Michael N. R. Ashfold[2*] and Vasilios G. Stavros[1*]

[1]Department of Chemistry, University of Warwick, Gibbet Hill Road, Coventry, CV4 7AL, UK

[2]School of Chemistry, University of Bristol, Cantock's Close, Bristol, BS8 1TS, UK

ABSTRACT: Oxybenzone is a common constituent of many commercially available sunscreens providing photoprotection from ultraviolet light incident on the skin. Femtosecond transient electronic and vibrational absorption spectroscopies have been used to investigate the non-radiative relaxation pathways of oxybenzone in cyclohexane and methanol after excitation in the UVA region. The present data suggest that the photoprotective properties of oxybenzone can be understood in terms of an initial ultrafast excited state enol → keto tautomerization, followed by efficient internal conversion and subsequent vibrational relaxation to the ground state (enol) tautomer.

TOC GRAPHIC

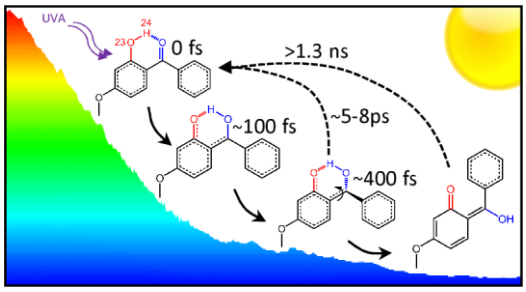

Keywords: *Oxybenzone, sunscreens, transient absorption spectroscopy, ultrafast photochemistry*

Sunscreens are used to act preemptively against an over exposure to ultraviolet (UV) radiation, which is known, for instance, to be responsible for the development of malignant melanomas.[1-3] Applied sunscreens work in addition to the body's delayed natural photoprotective mechanism: tanning.[4,5] Oxybenzone, termed OB hereon and shown in Figure 1 (labelled chelated enol), is an active ingredient present in many commercially available sunscreens, and has been the subject of many prior studies.[3,6-10] It displays broadband UV absorption (spanning the UVA and UVB regions; see Supporting Information (SI), Figure S1) and remains photostable after several hours,[11] but the mechanism by which it provides these beneficial properties remains to be established. There is also some controversy in observed adverse dermatological effects from skin-OB contact.[8,12-14] Elucidating the energy dissipation mechanism within OB could aid the selection and design of better sunscreens,[7] or suggest improvements in the use of OB itself. For example, recent studies have suggested that the adverse effects of skin-OB contact might be reduced through the use of zeolite encapsulation.[6,15]

Recent *ab initio* electronic structure studies suggested that

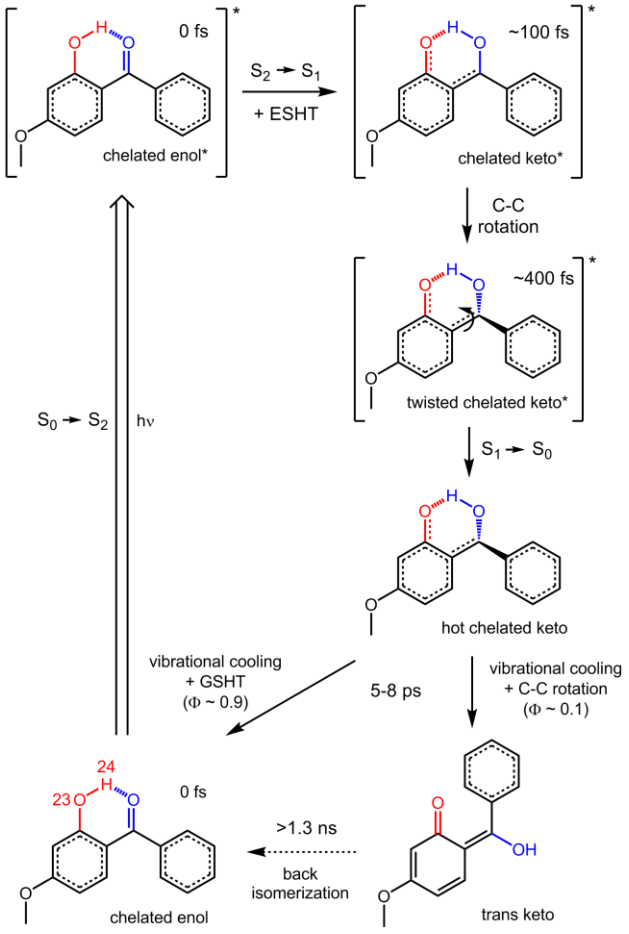

Figure 1. Overall proposed scheme of the energy dissipation mechanism of UVA excited OB. Key atoms involved in this mechanism are highlighted for clarity.

ultrafast dynamics may be key to understanding the efficiency of OB as a sunscreen.[10] These studies identified internal conversion (IC) via an electron-driven excited state hydrogen atom transfer (ESHT) mechanism as a plausible energy relaxation pathway, in concordance with studies in similar species containing hydrogen donor (OH)-acceptor (CO) sites in close proximity.[16,17] Recent studies have also revealed some probability of excited state OB molecules undergoing intersystem crossing (ISC) to long lived triplet states[9] and homolytic O–H bond fission to yield phenoxyl radicals.[18] The current evidence thus suggests that OB is photostable under UV irradiation (notwithstanding the undesirable minor ISC and O–H bond fission channels), but this cannot be confirmed whilst the OB excited state decay mechanism remains in question.

In this letter we use femtosecond pump-probe transient electronic (UV-visible) absorption spectroscopy (TEAS) and transient vibrational absorption spectroscopy (TVAS) methods to probe the ultrafast energy dissipation of OB following photoexcitation near the UVA absorption maximum, *ca.* 325 nm (3.81 eV). The dominant mechanism by which OB dissipates this energy is found to involve ultrafast excited state enol → keto tautomerization, followed by IC to reform the original chelated enol tautomer. A minor channel is also identified, attributed to formation of a longer lived trans keto product.

The Warwick TEAS setup,[19,20] employing 325 nm, 1–2 mJ cm^{-2} pump pulses and broadband white light continuum (340 to 675 nm) probe pulses was used to record the transient electronic absorption (TEA) spectra of OB in cyclohexane and methanol (10 mM), for a range of pump-probe time delays. These spectra are shown in Figures 2a and 2c, respectively. We start by considering the OB in cyclohexane data at very early pump-probe time delays (< 500 fs). The TEA spectra are dominated by two features: an intense, narrow peak centred at ~366 nm and a flat, broad absorption (425-575 nm) which tails off into the baseline by 650 nm. Based on the subsequent analysis (*vide infra*), we attribute this latter signal to OB excited state absorption (ESA). By 2 ps, most of the broad ESA feature in the TEA spectra has decayed away leaving the positive peak at 366 nm (indicated by the dashed line in Figure 2a), the identity of which we discuss below. A negative feature between 340 and 350 nm is also present which, by comparison with the static UV absorption spectrum of OB (see SI, Figure S1), we assign as a ground state bleach (GSB). By 50 ps, the 366 nm feature has decayed to the baseline, but the GSB does not fully recover and persists out to the maximum available pump-probe time delay (2 ns). Similar dynamics are found for OB in methanol with only a slight blue shifting of the observed features.

Quantitative insight into the dynamical processes involved in the TEA spectra can be gained by employing a global fitting procedure.[21,22] Two exponential functions are required in the global fit between 355 and 415 nm, which encompasses the absorption feature at 366 nm, to recover the data. For OB in cyclohexane, the lifetimes of the spectral features are τ_1 = 375 ± 13 fs and τ_2 = 7.8 ± 2.8 ps, see Figure 2b (red line). In methanol the corresponding lifetimes are τ_1 = 368 ± 13 fs and τ_2 = 4.9 ± 1.9 ps, see Figure 2d (red line). Further information on the global fits can be found in the SI (Figures S2-S4). The dynamics of the ESA feature beyond 415 nm are well described by a single exponential decay with a lifetime that closely mirrors the τ_1 value for OB in the corresponding solvent (see SI, Figure S4 for further information).

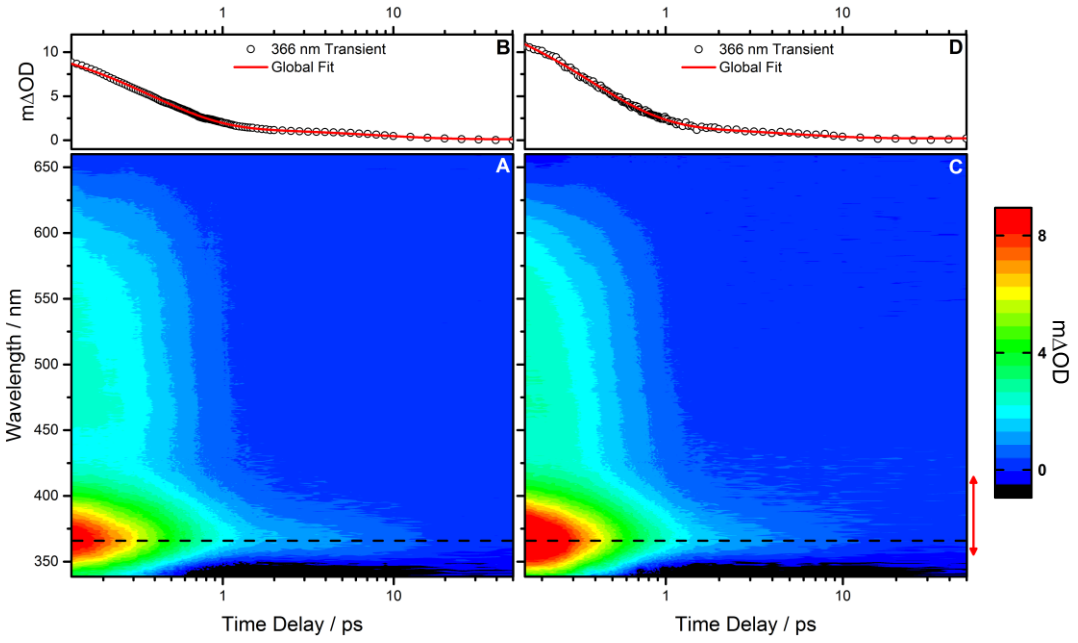

Figure 2. (A) Raw TEA spectra following 325 nm photoexcitation of OB in cyclohexane (in the form of a colour map indicating the change in optical density) showing the localised absorption centred at 366 nm (dashed line) and the broad absorption spanning the range 425-575 nm. (B) The transient signal extracted from the TEA spectra at 366 nm reveals two decay lifetimes τ_1 = 375 ± 13 fs and τ_2 = 7.8 ± 2.8 ps (determined from a global fit). Quoted errors correspond to 2 standard deviations (2σ). See SI for further details pertaining to the error analysis. Open circles represent experimental data whereas the red line is the global fit. (C) Raw TEA spectra following 325 nm photoexcitation of OB in methanol with corresponding transient (D). Lifetimes from a global fit are τ_1 = 368 ± 13 fs and τ_2 = 4.9 ± 1.9 ps. The red arrow denotes the range of the TEA spectra included in the global fit (355-415 nm).

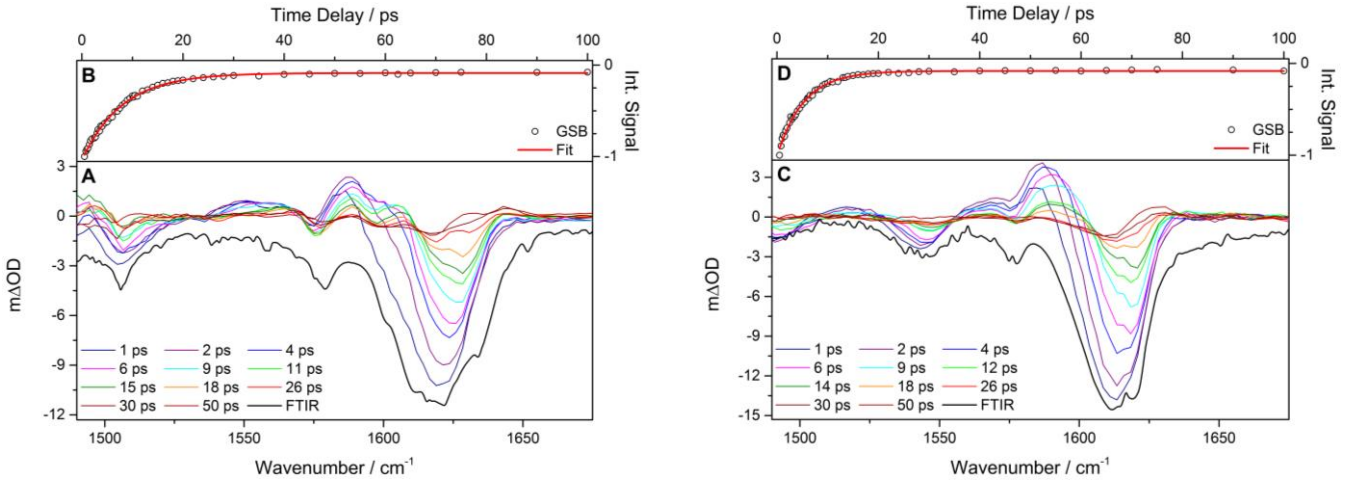

Figure 3. (A) Raw TVA spectra following 325 nm excitation of OB in cyclohexane. (B) Transient signal for the GSB recovery (open circles) calculated from the normalized numerical integration of the 1621 cm^{-1} GSB signal. Fitting this integrated signal with a single exponential function returns a lifetime for GSB recovery $\tau = 8.0 \pm 0.2$ ps (red line). (C) Raw TVA spectra for OB in methanol-d_4 with corresponding transient signal for GSB recovery (D), yielding a lifetime $\tau = 5.2 \pm 0.2$ ps. Quoted errors correspond to 2σ. The static FTIR spectra of OB in cyclohexane and in methanol-d_4 are shown as black lines in (A) and (C).

The Bristol TVAS setup,[23] employing 325 nm, 2 mJ cm^{-2} pump pulses with mid-IR probe pulses centred on 1580 cm^{-1} and pump-probe time delays up to 50 ps, was used to record TVA spectra of OB in cyclohexane (Figure 3a) and deuterated methanol (methanol-d_4, Figure 3c) at a concentration of 10 mM. We consider cyclohexane first. Several negative GSB features are observed at the earliest time delay (1 ps), the strongest of which is located at ~1620 cm^{-1} and matches well the static FTIR spectrum (Figure 3a, black line). A positive feature is also evident on the lower wavenumber edge of the strongest GSB; this feature decays and shifts to higher wavenumber within the first 10 ps (see SI, Figure S5 for further details). This temporal behaviour is characteristic of ultrafast formation of vibrationally hot ground state (S_0) OB molecules, which then relax through interaction with the solvent.[23] Returning to the ~1620 cm^{-1} GSB, numerical integration over the range of time delays yields the kinetic trace in Figure 3b, which is well described using a single exponential function (red line) with a lifetime of $\tau = 8.0 \pm 0.2$ ps. As was also seen in TEAS, the GSB does not recover fully on the timescale of the experiment, suggesting formation of a photoproduct with a quantum yield of ≥ 9 %. TVA spectra obtained following 325 nm photoexcitation of OB in methanol-d_4 reveal an analogous GSB at ~1610 cm^{-1}, with a lifetime of $\tau = 5.2 \pm 0.2$ ps (Figure 3d) that, again, recovers incompletely – implying a photoproduct quantum yield of ≥ 8 %. We note the good agreement between these τ values and the τ_2 time-constants from the TEAS data and return to discuss this correspondence later.

Recent *ab initio* electronic structure calculations on OB[10] assist our interpretation of the dynamical processes revealed in the TEAS and TVAS data, which we discuss with reference to the structures and mechanism in Figure 1. The calculations produce cuts through the potential energy surfaces (PESs) for the S_0, $S_1(1^1n\pi^*)$, $S_2(1^1\pi\pi^*)$ and $S_3(2^1\pi\pi^*)$ states of OB and reveal the availability of conical intersections by which population in the optically 'bright' S_2 state (formed as a result of 325 nm photoexcitation of the chelated enol) can be funnelled to the S_1 state (which is optically 'dark'). Following radiationless transfer to S_1, the calculations identify a barrierless ESHT pathway (along O_{23}–H_{24}, see Figure 1), involving necessary rotation about the central aliphatic C–C bond, that links the S_1 state to a conical intersection with the S_0 state. However, the resultant twisted chelated keto isomer (Figure 1) is not a stable species on S_0, and the local topography of the S_0 PES likely provides a driving force to regenerate the original stable chelated enol isomer through ground state hydrogen atom transfer (GSHT), which is cooled *via* vibrational energy transfer (VET) to the solvent bath.[24-26]

The TEAS measurements identify three dynamical features. The TEA spectra highlight two of these, which, from the fitting of the 366 nm absorption maximum, reveal a short (τ_1) and a longer-time (τ_2) process. The third feature is an apparent flat maximum close to time-zero in the transients shown in Figures 2b and 2d, which persists for ~100 fs (see SI, Figure S3). Guided by the *ab initio* calculations,[10] we try to rationalise these features. The signal plateau around time-zero, which we are unable to resolve within our instrument response (~100 fs), is attributed to a combination of ultrafast IC from the photoexcited S_2 state to S_1, and ballistic ESHT on the S_1 state. After ESHT to form the chelated keto species, slower rotation about the central C–C bond can occur, enabling IC back to the S_0 state through an S_1/S_0 conical intersection at the twisted chelated keto structure (see Figure 1). We associate τ_1 with this subsequent twisting and IC process (the timescale is sensibly consistent with that derived for enol → keto tautomerism in similar systems that require a twisted ESHT[27-29]). Two caveats are in order here. First, we cannot rule out the alternative possibility that τ_1 represents simultaneous (or concerted) H-atom transfer *and* C–C twisting, prior to IC from S_1 to S_0, in which case the short lived, flat absorption transient would most likely be attributable to IC from S_2 to S_1. Second, given the low frequency of the torsional mode, some fraction of the molecular ensemble will already be in the correct (or a more correct) geometry to pass through the S_1/S_0 conical intersection. τ_1 reflects the dynamics of the overall molecular ensemble. After

IC to form hot S_0 molecules, GSHT can regenerate the original chelated enol structure, which is then quenched by VET to the solvent. We associate τ_2 with this final VET mediated cooling process. Support for this assignment comes from the evident small red-shift of the UVA absorption maximum of OB to ~366 nm (*cf*. the static UV absorption of OB, SI Figure S1) – the expected characteristic of vibrationally hot S_0 OB molecules.[30] The TVAS measurements support this conclusion: given the ultrashort (τ_1) lifetime of photoexcited OB molecules in both solvents, the recovery of the GSB features in TVAS will report the rate of vibrational cooling of hot S_0 OB molecules, as described for other systems.[23] Importantly, the GSB recovery timescales from TVAS (τ) mirror closely the τ_2 values assigned to VET driven cooling in TEAS. Further, both τ and τ_2 are solvent dependent; the extracted lifetimes for methanol are consistently shorter than in cyclohexane, implying higher VET efficiencies in methanol-OB than in cyclohexane-OB. Such is fully consistent with prior expectations that the interaction of OB with a more strongly interacting (polar) solvent will promote a higher rate of VET.[26]

As noted above, a small fraction (~10 %) of the GSB does not recover in either solvent, which is a tell-tale sign of some form of extended dynamics or photoproduct formation. Such a conclusion is reinforced by the appearance of a new absorption feature centred at 1640 cm^{-1} in cyclohexane (1630 cm^{-1} in methanol-d_4) in the TVA spectra recorded at extended time-delays. Both the residual GSB and this new absorption feature are evident in the TVA spectra shown in Figure 4a for the case of OB in cyclohexane at two pump-probe delays, 50 and 200 ps (see Figure S7 in SI for the corresponding TVA spectra following excitation of OB in methanol-d_4). Possible carriers of this new feature have been explored using density functional theory at the B3LYP/6-311+G** level within the Gaussian03 computational package[31] to determine gas-phase harmonic vibrational wavenumbers for the chelated enol and a number of possible photoproduct structures/triplet states (see SI, Figures S6-S8 for further details). We specifically focus on vibrations that fall within the probe window of interest. The calculations for the chelated enol return a number of vibrations in the relevant wavenumber range, the strongest of which is not the C=O stretch but a ring stretch mode of the methoxyphenol moiety (1668 cm^{-1}), which is responsible for the GSB observed in the TVA spectra in both solvents (Figures 3a and 3c).

Given previous condensed phase observations,[9] triplet state formation must be one possible assignment for the emerging positive feature in the TVA spectra, but comparison with calculated triplet state spectra for several different OB structures/isomers tends to rule out this suggestion (see SI, Figure S8). Based on the recent *ab initio* electronic structure calculations[10] and findings from experimental studies of twisted ESHT mechanisms in related systems,[27-29] we propose an alternative assignment for the signal carrier of this new feature at ~1640 cm^{-1}. As discussed above, rotation about the central aliphatic C–C bond is essential for enabling access to the S_1/S_0 conical intersection at the twisted chelated keto geometry (Figure 1). As with similar model systems,[27-29] momentum in this torsional motion may in principle enable further rotation about the C–C bond, after formation of the hot chelated keto species on S_0, to yield a trans keto photoproduct (Figure 1), rather than GSHT back to the chelated enol. Once formed, the trans keto species may then undergo vibrational cooling. To confirm the above mechanism, we have calculated harmonic vibrational wavenumbers for the two possible (OH group) rotamers of the trans keto species and a number of other theoretically possible photoproduct structures (see SI),[10] and conclude that the emergent absorption feature is most likely attributable to a C=O stretch of the trans keto tautomer rather than any other photoproduct. Figure 4b shows the predicted

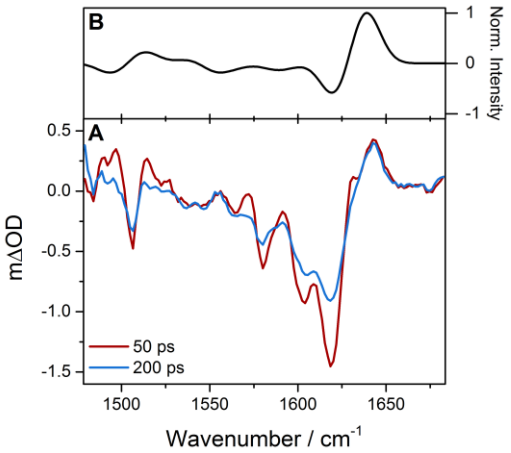

Figure 4. (A) TVA spectra measured following 325 nm excitation of OB in cyclohexane at pump-probe time delays of 50 ps and 200 ps. (B) Difference spectrum derived from the harmonic wavenumbers and IR transition strengths for the chelated enol-OB and 'trans' keto-OB tautomer. See text and SI for further details.

difference absorption spectrum assuming formation of this trans keto product. This spectrum was generated as a sum of the calculated bleach and absorption spectra of the chelated enol and trans keto species, respectively (see SI for further details). As is evident from Figure 4, the calculated and experimental spectral profiles are in very reasonable agreement. Assigning the emergent feature to a trans keto product provides further support for the conclusion that photoexcited OB molecules decay primarily via a twisted ESHT mechanism. We are unable to obtain kinetic information relating to the formation of the trans keto photoproduct as the feature is too heavily masked by the stronger GSB signal. Nonetheless, our attribution of trans keto product signal at pump-probe time delays as long as 1.3 ns would imply that, although ~90 % of the excited state population reverts to the chelated enol, the remaining ~10 % is trapped in the higher energy trans keto form over (at least) a nanosecond timescale.

We now revisit the possible importance of excited state O–H bond fission and phenoxyl radical formation, which Ignasiak *et al.*[18] suggested a possible explanation for the incomplete signal recovery in their TEA spectra. The present study corroborates other aspects of their recent study, but careful inspection of the present TEA data (*e.g.* Figure 2) at wavelengths ~400 nm, where such phenoxyl radicals show a well-documented absorption,[32,33] reveals no such signature. The present measurements thus suggest that O–H bond fission is an insignificant photoproduct channel (at least within our signal-to-noise) and that the incomplete signal recovery[18] might more likely be attributable to a trans keto photoproduct. However, we also note differences in the pulse energy and photo-

excitation wavelengths used in the two studies (10 μJ/pulse, 340 nm in ref. 18, *cf.* < 1 μJ/pulse and 325 nm in the present work) and suggest that additional pulse energy and/or wavelength studies might be necessary to check that such factors do not affect the detailed excited state dynamics of OB.

We close our discussion by briefly considering the role of OB in a real sunscreen environment and relate this to the present findings. Sunscreens are multicomponent systems, which include both organic and inorganic components in both polar and non-polar solvents. Trying to elucidate the energy dissipation mechanisms within the entire mixture is intractable. The bottom-up approach utilized here, where we study the energy dissipation mechanism of OB in a polar and non-polar solvent, is more tractable and may serve as a stimulus for future investigations. For instance, what happens when the complexity of the system is increased by introducing a second sunscreen constituent? Are the photoprotection properties afforded by the mix greater than the sum of the individual parts? Both experiment and theory will surely be required to answer these, and many other, questions in the field of sunscreen science.

To conclude we have determined two ultrafast relaxation processes by which photoexcited OB molecules revert to (predominantly) the ground state, where they are available to continue to absorb UV radiation. We suggest that the mechanism by which OB dissipates energy following UV excitation involves ultrafast excited state enol → keto tautomerization, followed by two (IC) relaxation processes to reform the original chelated enol tautomer.

ASSOCIATED CONTENT

Supporting Information

UV-visible spectrum of OB in cyclohexane and methanol. Global fits to the TEA spectra. Vibrational cooling dynamics from the TVA spectra. Calculated triplet/photoproduct TVA difference spectra. Further experimental details. This information is available free of charge via the Internet at http://pubs.acs.org/.

AUTHOR INFORMATION

Corresponding Author

*Email: v.stavros@warwick.ac.uk, mike.ashfold@bris.ac.uk

Author Contributions

‡These authors contributed equally.

ACKNOWLEDGMENTS

The authors are grateful to Prof. Philipp Kukura (Oxford) and Dr Adam Chatterley (UC Berkeley) for helpful discussions. L.A.B. thanks the Engineering and Physical Sciences Research Council for providing a studentship under grant EP/F500378/1, through the Molecular Organisation and Assembly in Cells DTC. M.D.H. thanks the University of Warwick for an EPSRC studentship. S.E.G. thanks the Warwick Institute of Advanced Study for postdoctoral funding. The Bristol work was supported by the European Research Council through ERC Advanced Grant 290966 CAPRI and EPSRC via Programme Grant EP/L005913. G.M.R. thanks the Ramsay Memorial Trust for a Fellowship and Prof. Martin Paterson (Heriot-Watt) for use of his computational facilities. V.G.S. thanks the EPSRC for an equipment grant (EP/J007153) and the Royal Society for a University Research Fellowship.

REFERENCES

(1) Ortonne, J. P. Photoprotective Properties of Skin Melanin. *Br. J. Dermatol.* **2002**, *146*, 7-10.

(2) Mason R. S.; Reichrath, J. Sunlight, Vitamin D and Skin Cancer. *Anticancer Agents Med. Chem.* **2013**, *13*, 83-97.

(3) González, S.; Fernández-Lorente, M.; Gilaberte-Calzada, Y. The Latest on Skin Photoprotection. *Clin. Dermatol.* **2008**, *26*, 614-626.

(4) Brenner, M.; Hearing, V. J. The Protective Role of Melanin Against UV Damage in Human Skin. *Photochem. Photobiol.* **2008**, *84*, 539-549.

(5) Agar, N.; Young, A. R. Melanogenesis: A Photoprotective Response to DNA Damage? *Mutat. Res.* **2005**, *571*, 121-132.

(6) Forestier, S. Rationale for Sunscreen Development. *J. Am. Acad. Dermatol.* **2008**, *58*, S133-S138.

(7) Stavros, V. G. Photochemistry: A Bright Future for Sunscreens. *Nature Chem.* **2014**, *6*, 955-956.

(8) Burnett, M. E.; Wang, S. Q. Current Sunscreen Controversies: A Critical Review. *Photodermatol. Photoimmunol. Photomed.* **2011**, *27*, 58-67.

(9) Kumasaka, R.; Kikuchi, A.; Yagi, M. Photoexcited States of UV Absorbers, Benzophenone Derivatives. *Photochem. Photobiol.* **2014**, *90*, 727-733.

(10) Karsili, T. N. V.; Marchetti, B.; Ashfold, M. N. R.; Domcke, W. *Ab Initio* Study of Potential Ultrafast Internal Conversion Routes in Oxybenzone, Caffeic Acid, and Ferulic Acid: Implications for Sunscreens. *J. Phys. Chem. A.* **2014**, *118*, 11999-12010.

(11) Serpone, N.; Salinaro, A.; Emeline, A. V.; Horikoshi, S.; Hidaka, H.; Zhao, J. An *In Vitro* Systematic Spectroscopic Examination of the Photostabilities of a Random Set of Commercial Sunscreen Lotions and their Chemical UVB/UVA Active Agents. *Photochem. Photobiol. Sci.* **2002**, *1*, 970-981.

(12) Ambrogi, V.; Latterini, L.; Marmottini, F.; Tiralti, M. C.; Ricci, M. Oxybenzone Entrapped in Mesoporous Silicate MCM-41. *J. Pharm. Innov.* **2013**, *8*, 212-217.

(13) Lodén, M.; Beitner, H.; Gonzalez, H.; Edström, D.; Akerström, U.; Austad, J.; Buraczewska-Norin, I.; Matsson, M.; Wulf, H. Sunscreen Use: Controversies, Challenges and Regulatory Aspects. *Br. J. Dermatol.* **2011**, *165*, 255-262.

(14) Sambandan, D. R.; Ratner, D. Sunscreens: An Overview and Update. *J. Am. Acad. Dermatol.* **2011**, *64*, 748-758.

(15) Chrétien, M. N.; Heafey, E.; Scaiano, J. C. Reducing Adverse Effects from UV Sunscreens by Zeolite Encapsulation: Comparison of Oxybenzone in Solution and in Zeolites. *Photochem. Photobiol.* **2010**, *86*, 153-161.

(16) Perun, S.; Sobolewski, A. L.; Domcke, W. Role of Electron-Driven Proton-Transfer Processes in the Excited-State Deactivation of the Adenine-Thymine Base Pair. *J. Phys. Chem. A.* **2006**, *110*, 9031-9038.

(17) Sobolewski, A. L.; Domcke, W.; Hättig, C. Tautomeric Selectivity of the Excited-State Lifetime of Guanine/Cytosine Base Pairs: The Role of Electron-Driven

Proton-Transfer Processes. *Proc. Natl. Acad. Sci. U.S.A.* **2005**, *102*, 17903-17906.

(18) Ignasiak, M. T.; Houée-Levin, C.; Kciuk, G.; Marciniak, B.; Pedzinkski, T. A Reevaluation of the Photolytic Properties of 2-Hydroxybenzophenone-Based UV Sunscreens: Are Chemical Sunscreens Inoffensive? *ChemPhysChem.* **2015**, *16*, 628-633.

(19) Greenough, S. E.; Horbury, M. D.; Thompson, J. O. F.; Roberts, G. M.; Karsili, T. N. V.; Marchetti, B.; Townsend, D.; Stavros, V. G. Solvent Induced Conformer Specific Photochemistry of Guaiacol. *Phys. Chem. Chem. Phys.* **2014**, *16*, 16187-16195.

(20) Greenough, S. E.; Roberts, G. M.; Smith, N. A.; Horbury, M. D.; McKinlay, R. G.; Zurek, J. M.; Paterson, M. J.; Sadler, P. J.; Stavros, V. G. Ultrafast Photo-Induced Ligand Solvolysis of *cis*-$[Ru(bipyridine)_2(nicotinamide)_2]^{2+}$: Experimental and Theoretical Insight into its Photoactivation Mechanism. *Phys. Chem. Chem. Phys.* **2014**, *16*, 19141-19155.

(21) Chatterley, A. S.; West, C. W.; Stavros, V. G.; Verlet, J. R. R. Time-Resolved Photoelectron Imaging of the Isolated Deprotonated Nucleotides. *Chem. Sci.* **2014**, *5*, 3963-3975.

(22) Chatterley, A. S.; West, C. W.; Roberts, G. M.; Stavros, V. G.; Verlet, J. R. R. Mapping the Ultrafast Dynamics of Adenine onto its Nucleotide and Oligonucleotides by Time-Resolved Photoelectron Imaging. *J. Phys. Chem. Lett.* **2014**, *5*, 843-848.

(23) Roberts, G. M.; Marroux, H. J. B.; Grubb, M. P.; Ashfold, M. N. R.; Orr-Ewing, A. J. On the Participation of Photoinduced N–H Bond Fission in Aqueous Adenine at 266 and 220 nm: A Combined Ultrafast Transient Electronic and Vibrational Absorption Spectroscopy Study. *J. Phys. Chem. A.* **2014**, *118*, 11211-11225.

(24) Harris, S. J.; Murdock, D.; Zhang, Y.; Oliver, T. A. A.; Grubb, M. P.; Orr-Ewing, A. J.; Greetham, G. M.; Clark, I. P.; Towrie, M.; Bradforth, S. E.; Ashfold, M. N. R. Comparing Molecular Photofragmentation Dynamics in the Gas and Liquid Phases. *Phys. Chem. Chem. Phys.* **2013**, *15*, 6567-6582.

(25) Aßmann, J.; Kling, M.; Abel, B. Watching Photoinduced Chemistry and Molecular Energy Flow in Solution in Real Time. *Angew. Chem. Int. Ed.* **2003**, *42*, 2226-2246.

(26) Owrutsky, J. C.; Raftery, D.; Hochstrasser, R. M. Vibrational Relaxation Dynamics in Solutions. *Annu. Rev. Phys. Chem.* **1994**, *45*, 519-555.

(27) Verma, P. K.; Koch, F.; Steinbacher, A.; Nuernberger, P.; Brixner, T. Ultrafast UV-Induced Photoisomerization of Intramolecularly H-Bonded Symmetric β-Diketones. *J. Am. Chem. Soc.* **2014**, *136*, 14981-14989.

(28) Verma, P. K.; Steinbacher, A.; Koch, F.; Nuernberger, P.; Brixner, T. Monitoring Ultrafast Intramolecular Proton Transfer Processes in an Unsymmetric β-Diketone. *Phys. Chem. Chem. Phys.* **2015**, *17*, 8459-8466.

(29) Barbatti, M.; Aquino, A. J. A..; Lischka, H.; Schriever, C.; Lochbrunner, S.; Riedle, E. Ultrafast Internal Conversion Pathway and Mechanism in 2-(2'-hydroxyphenyl)benzothiazole: A Case Study for Excited-State Intramolecular Proton Transfer Systems. *Phys. Chem. Chem. Phys.* **2009**, *11*, 1406-1415.

(30) Nosenko, Y.; Wiosna-Salyga, G.; Kunitski, M.; Petkova, I.; Singh, A.; Buma, W. J.; Thummel, R. P.; Brutschy, B.; Waluk, J. Proton Transfer with a Twist? Femtosecond Dynamics of 7-(2-pyridyl)-indole in Condensed Phase and in Supersonic Jets. *Angew. Chem. Int. Ed.* **2008**, *47*, 6037-6040.

(31) Frisch, M. J.; *et al.*, *Gaussian 03;* Gaussian Inc.: Wallingford, CT, 2004.

(32) Land, E. J.; Porter, G.; Strachan, E. Primary Photochemical Processes in Aromatic Molecules. *Trans. Faraday Soc.* **1961**, *57*, 1885-1893.

(33) Lind, J.; Shen, X.; Eriksen, T. E.; Merényi, G. The One-Electron Reduction Potential of 4-Substituted Phenoxyl Radicals in Water. *J. Am. Chem. Soc.* **1990**, *112*, 479-482.